

# Water Resources Research

## RESEARCH ARTICLE

10.1029/2019WR024875

### Key Points:

- A novel numerical model is proposed to simulate accretion and natural consolidation of tidal marshes
- The feedbacks between surface and subsurface processes are investigated through a coupling approach
- Compaction of the marsh body crucially affects the landform elevation and, in turn, its resilience to relative sea level rise

### Correspondence to:

C. Zoccarato,  
claudia.zoccarato@unipd.it

### Citation:

Zoccarato, C., DaLio, C., Tosi, L., & Teatini, P. (2019). A coupled biomorpho-geomechanical model of tidal marsh evolution. *Water Resources Research*, 55. <https://doi.org/10.1029/2019WR024875>

Received 30 JAN 2019

Accepted 8 SEP 2019

Accepted article online 9 OCT 2019

## A Coupled Biomorpho-Geomechanical Model of Tidal Marsh Evolution

C. Zoccarato<sup>1</sup> , C. Da Lio<sup>2</sup>, L. Tosi<sup>3,4</sup> , and Pietro Teatini<sup>1,4</sup> 

<sup>1</sup>Department of Civil, Environmental and Architectural Engineering, University of Padova, Padua, Italy, <sup>2</sup>Institute of Marine Sciences, National Research Council, Venice, Italy, <sup>3</sup>Institute of Geosciences and Earth Resources, National Research Council, Padua, Italy, <sup>4</sup>UNESCO Land Subsidence International Initiative,

**Abstract** Ecogeomorphic characteristics of tidal marshes are strongly related to their elevation with respect to the mean sea level. Predicting the long-term evolution and resilience of such ecosystems in times of rapid natural and anthropogenic climate changes is of critical importance. The notion that the tidal marsh elevation is the result of feedbacks between vegetation dynamics, sediment fluxes, natural consolidation, and sea-level changes is widely recognized. However, the interaction of these processes has been poorly investigated until now. This contribution aims at presenting a novel numerical model to simulate the above-surface and subsurface coupled dynamics of a tidal landscape in a 2-D-framework, with the relative sea-level rise (RSLR) acting as an external stressor. A biomorphological model is used to compute deposition fluxes, which depends on topography and availability of organic/inorganic sediments. The outcome is used as forcing term in a physically based geomechanical model to simulate the consolidation of the marsh body that, in turn, influences sediment fluxes by acting on the platform elevation. The results demonstrate how compaction of the marsh body can crucially affect the resilience of tidal landforms to RSLR accelerations. With normal sediment concentration in coastal waters ( $10 < C_0 < 100$  mg/l), if minerogenic (stiff) deposits prevail, a tidal marsh is capable of maintaining its elevation relative to mean sea level independently of RSLR (at least up to 10 mm/yr). When the marsh is composed of a large percentage of more compressible organic matter, the landform resilience is much more dependent on RSLR, implying higher vulnerability with respect to future climate changes.

### 1. Introduction

Tidal marshes occupy the upper margins of the intertidal landscape and they play an important role for the entire ecosystem because they protect coastal shores from storm waves, act as sediment trapping zones, store large CO<sub>2</sub> amounts, preserving biodiversity, facilitate organic and bacterial production, represent favorable habitats to the reproduction of many species of birds, and provide many recreational opportunities (Adam, 1990; Chmura et al., 2012; Costanza et al., 1997).

The resilience of such ecosystems is strictly connected to their height with respect to mean sea level (msl). The loss of relative elevation because of sea-level rise, land subsidence, erosion, or sedimentation decrease can cause a marsh to shift to a different stable state, for example, a tidal flat (Marani et al., 2010). The prediction of the long-term evolution of tidal marsh elevation is of great importance in times of rapid natural and anthropogenic climate changes. However, physically based models that couple processes occurring above (inorganic sediment deposition and production of organic matter) and below (shallow compaction and regional tectonic) ground surface are still lacking.

Over the past decades, a great effort has been made to devise mathematical tools predicting the tidal landscape evolution (e.g., D'Alpaos et al., 2012; Marani et al., 2007; Morris, 2006; Murray et al., 2008). The available biomorphodynamic models take into account physical and biological processes occurring on the marsh platform including water fluxes, sediment transport, vegetation dynamics, and their mutual interactions (Fagherazzi et al., 2012). It is well established that hydrodynamic and morphodynamic processes interplay with biomass production due to the presence of halophytic vegetation species (Day et al., 1999; Da Lio et al., 2013; Kirwan & Murray, 2007) and contribute in a two-way feedback dynamic determining the salt-marsh ecosystem formation and resilience (D'Alpaos & Marani, 2016). In addition, sea-level variations crucially influence the delicate balance of the tidal wetlands by acting on many processes such as mineral

deposition rates, productivity of marsh macrophytes, decay of organic matter, and marsh erosion (French, 2006; Mariotti & Fagherazzi, 2010; Morris et al., 2002; Mudd et al., 2009).

This is the reason why, from a geological perspective, tidal marsh sediments are considered (paleo-)sea-level proxies and provide precise and near-continuous reconstructions of relative sea level over the last millennia (Brain et al., 2017). Deriving the past sea-level evolution from a marsh stratigraphy is challenging. Because of the large porosity typical of newly formed landforms, shallow deposits experience a significant consolidation (Allen, 1999; Cahoon et al., 2002; Jankowski et al., 2017) with the ongoing compaction at a certain depth depending on the load of the overlying more recent deposits (Brain et al., 2012). Autocompaction is potentially included in the vertical marsh growth model of French (1993) but eventually using a precompacted organic matter. Compaction is assumed as a forcing function in Chmura et al. (1992), with empirical relationships implemented in Allen (1999), Callaway et al. (1997), and Rybczyk et al. (1998). More advanced 1-D compression models were proposed by Paul and Barras (1998), Massey et al. (2006), and Brain et al. (2011), also associated with the solution of the 1-D groundwater flow equation based on Darcy's law (e.g., Pizzuto & Schwendt, 1997) and applied to quantify compaction in coastal marshes. Other numerical models were developed to include deep natural processes such as isostatic subsidence (Wolstencroft et al., 2014). More recently, Zoccarato and Teatini (2017) proposed a physically based modeling approach where a 2-D framework was established to accurately describe the below-ground geomechanical processes determining the wetland surface evolution.

The approaches presented above are either purely biomorphological or purely hydro-geomechanical, with simplified known forcing factors such as land subsidence and sedimentation rates for the former and the latter approach, respectively. This contribution aims at providing a first attempt to investigate the evolution of a tidal marsh considered as a whole (surface and above-surface coupled systems). Its shape (elevation) depends on the intrinsic hydro-geomechanical properties of the porous body and the physical and biological processes occurring on its upper surface. We present a novel numerical model to simulate the above-surface and subsurface coupled dynamics of a tidal landscape in a 2-D framework. We use the description of the main biomorphological processes as proposed by (Marani et al., 2010) and (D'Alpaos et al., 2012) to compute the deposition rates, which depend on topography and availability of organic/inorganic sediments. The outcome is then used as a forcing term of the geomechanical model by Zoccarato and Teatini (2017), which simulates the consolidation process properly considering the large deformations typical of shallow soft deposits, and including the relative sea-level rise (deep subsidence plus eustatic sea-level rise) as an external forcing factor. The compaction term, in turn, influences the sediment deposition fluxes by controlling the accommodation space and, therefore, acting on the surface elevation.

The paper is organized as follows. The modeling framework is initially presented with a review of the surface and subsurface modules and an in-depth discussion on their coupling. Then, the biomorpho-geomechanical model is initially applied to a simplified test case to (i) investigate the marsh evolution in relation to the variation of the main input parameters, that is, the geomechanical properties of the soil, the sediment concentration in the surface water, the relative sea-level rise, and biomass production, and (ii) highlight the feedbacks between consolidation and biomorphological marsh characteristics. An application to a realistic test case follows, using a representative data set of the Venice Lagoon, Italy. Finally, a discussion section and the conclusions analyze the results and draw the main findings.

## 2. Modeling Framework

The biomorpho-geomechanical model presented here is delineated in the context of the long-term evolution of tidal marshes even though the framework might be applied to other transitional environments (e.g., a tidal flat or a delta front) where the same main assumptions hold.

The change of marsh thickness  $z_t(x, t)$  is the result of the above- and below-ground processes depicted in Figure 1:

$$\frac{d[z_t(x, t)]}{dt} = Q_s(x, t) + Q_o(x, t) - \Delta z_t(x, t), \quad (1)$$

where  $Q_s(x, t)$  and  $Q_o(x, t)$  are the inorganic and organic deposition rates on the marsh surface and  $\Delta z_t(x, t)$  is the marsh thickness variation due to compaction. Hence, the elevation of the tidal platform relative to the

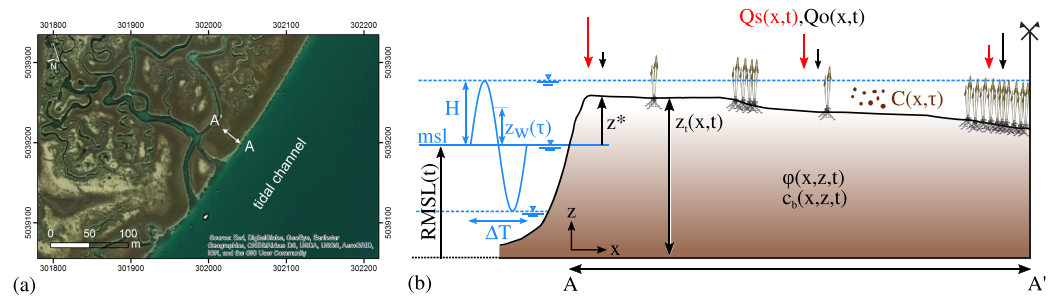


**Figure 1.** (a) Satellite image of a tidal marsh environment in the Venice Lagoon, Italy and (b) conceptual illustration of the tidal marsh cross-section A-A'. The inorganic and organic deposition rates  $Q_s(x, t)$  and  $Q_o(x, t)$  are represented by red and black arrows, respectively, whereas  $C(x, \tau)$  is the local instantaneous suspended sediment concentration within the water column. In a tidal cycle interval, the actual water level  $z_w(\tau)$  fluctuates over the marsh top within the range  $\text{msl} \pm H$ , where  $\text{msl}$  represents the actual mean sea level. The marsh is characterized by the soil oedometric compressibility  $c_b$  and the soil matrix porosity  $\phi$ , which are functions of  $\sigma_z(x, z, t)$ , thus they vary with the thickness  $z_t(x, t)$ . Note that  $\tau$  and  $t$  represent the timescales of the processes occurring at tidal and consolidation scales (Figure 2).

actual  $\text{msl } z^*(x, t)$  reads

$$z^*(x, t) = z_t(x, t) - \text{RMSL}(t) \quad (2)$$

with  $\text{RMSL}(t)$  the relative  $\text{msl}$  defined as

$$\text{RMSL}(t) = \int_0^t \text{RSLR}(s) ds, \quad (3)$$

where the relative sea-level rise (RSLR) is the sum of the sea-level rise and the land subsidence of the Pleistocene–Holocene boundary, generally representing the marsh bottom.

Before a detailed description of the modules used to quantify the various contributions, it is worth mentioning that the simulated processes occur at different timescales that must be properly accounted for. In Figure 2, three temporal scales are represented. The macro-scale reflects the long-term evolution of the marsh over the time span between  $t_0$  and  $t_f$ . A temporal discretization  $\Delta t$  is used. This is the typical timescale of the hydro-geomechanical processes, during which consolidation plays the main role. The biomorphological processes are simulated within each  $\Delta t$ . From time  $t_k$  to  $t_{k+1}$ , the biomorphological changes occurring in the system are computed as cumulative values of the processes taking place at the tidal timescale  $\Delta T$ . In turn, within a period  $\Delta T$ , the time-discretization  $\Delta \tau$  is used to simulate the sediment transport and deposition processes varying within the interval  $[t_k + n\Delta T] - [t_k + (n+1)\Delta T]$ , with  $n$  the number of tidal periods in the range  $t_{k+1} - t_k$ . The coupling of the temporal scales is further detailed in section 2.3.

### 2.1. Biomorphological Module

Let us consider a marsh transect AA' orthogonal to the nearest tidal channel (Figure 1). The total sediment deposition rate at a distance  $x$  from the marsh edge and time  $t$  reads (Da Lio et al., 2013)

$$\omega(x, t) = Q_s(x, t) + Q_o(x, t). \quad (4)$$

We neglect sediment capture by marsh vegetation, consistently with recent findings by Da Lio et al. (2013) and Mudd et al. (2010), who showed that particle settling largely dominates capture for flow velocities commonly observed in tidal marshes (up to 0.05 m/s). We also neglect erosion of the marsh surface because neither tidal currents nor wind-waves usually produce bottom shear stresses high enough to erode the vegetated marsh top. The presence of halophytes damp waves (Augustin et al., 2009) protects the surface against erosion by currents (Christiansen et al., 2001).

In equation (4),  $Q_s(x, t)$  is computed as a tidally-average accretion rate (Da Lio et al., 2013):

$$Q_s(x, t) = \frac{w_s}{\rho_b} \frac{n_T}{\Delta T} \int_{\Delta T} C(x, \tau) d\tau, \quad (5)$$

where  $C(x, \tau)$  is the local instantaneous suspended-sediment concentration (SSC) within the water column,  $\Delta T$  is the tidal period over which averaging is performed,  $n_T$  is the number of tidal periods in a considered

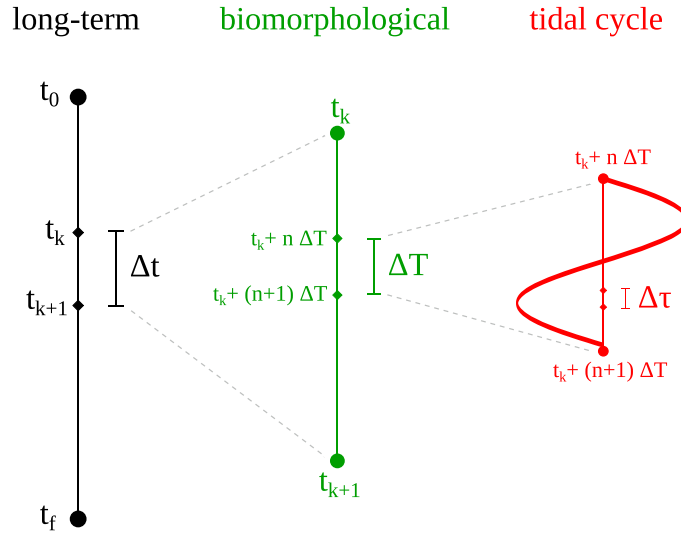


**Figure 2.** Temporal scales characteristic of the modeling framework. The simulated processes occur over a long-term scale (e.g., thousands of years), a biomorphological scale (e.g., 1 year), and at the scale of the tidal cycle (e.g., 12 hr by using a semidiurnal tidal cycle).

discretization interval  $\Delta t$  (e.g., a year),  $w_s$  is the settling velocity,  $\rho_b = \rho_s(1 - \phi_0)$  is the bulk density with  $\rho_s$  the soil grain density, and  $\phi_0$  is the porosity of the deposited soil on the marsh surface. Equation (5) shows that  $Q_s(x, t)$  can be determined only once the local and instantaneous SSC is known along the  $x$ -coordinate of the transect. To this aim, we consider the following advection-dispersion equation along the transect, solved over the timescale of a single tidal cycle  $\Delta T$  (Da Lio et al., 2013):

$$\frac{\partial(yC)}{\partial\tau} + \frac{\partial}{\partial x} \left( uCy - k_d y \frac{\partial C}{\partial x} \right) = -w_s C, \quad (6)$$

where  $y(x, \tau) = z_w(\tau) - z^*(x, t)$  is the local instantaneous water depth,  $z_w(\tau)$  is the spatially uniform instantaneous tidal elevation with respect to the local msl,  $k_d$  is the dispersion coefficient, and  $u(x, \tau)$  is the local instantaneous water advective velocity.  $z_w(\tau)$  is obtained by assuming a semidiurnal sinusoidal fluctuation of the tidal level, that is,  $z_w(\tau) = -H \cdot \cos(2\pi\tau/T)$  with  $H$  the tidal amplitude.

The flow field,  $u(x, \tau)$ , is determined from the continuity equation as follows:

$$\frac{\partial y}{\partial\tau} + \frac{\partial(yu)}{\partial x} = 0 \quad (7)$$

Equations (6) and (7) are separately solved through a finite-volume numerical method over a tidal cycle (Da Lio et al., 2013). It is worth noting that because the marsh topography usually evolves on a timescale much longer than the water motion does, the solution of the hydrodynamic field (Equation (7)) and of sediment transport dynamics (Equation (6)) during a tidal cycle is decoupled from the morphological evolution.

The contribution  $Q_o(x, t)$  within a time interval  $\Delta t$  (equation (4)) depends on the biomass production rate  $B(x, t)$ .  $B(x, t)$  is a function of the vegetation species colonizing the location  $x$  along the transect. It may be assumed that vegetation adapts to changes in elevation very quickly (D'Alpaos et al., 2012; Mudd et al., 2004) compared to typical morphological timescales (several years). Under this hypothesis,  $B(x, t)$  instantaneously adapts to soil elevation and it is solely a function of  $z^*$ . Following D'Alpaos et al. (2012) and Da Lio et al. (2013), the organic accretion rate  $Q_o(x, t)$  reads

$$Q_o(x, t) = \gamma_b B(z^*) = \gamma_b B_0 f(z^*), \quad (8)$$

where the coefficient  $\gamma_b$  incorporates both typical vegetation characteristics and the density of the produced organic soil,  $B_0$  is the maximum biomass density of a fully vegetated marsh, and  $f(z^*)$  is a fitness function ( $0 \leq f(z^*) \leq 1$ ) describing how biomass production varies as a function of the marsh elevation relative to the actual msl, summing up local environmental stressors such as salinity and sediment aeration (Blum & Christian, 2013; Da Lio et al., 2013; Marani et al., 2010; Mudd et al., 2009). Considering a *Spartina*-dominated

environment,  $f(z^*)$  is a linearly decreasing function of  $z^*$ , with  $B = B_0$  if  $z^* = 0$  and  $B = 0$  if  $z^* = H$  (D'Alpaos et al., 2012). Biomass productivity is the highest at  $z^* = 0$  and vanishes at  $z^* = H$ . If the marsh surface is below the msl,  $B = 0$ , that is, the landform shifts from a marsh to a tidal flat with no vegetation on its surface.

## 2.2. Geomechanical Module

As new sediments deposit over the tidal marsh surface, the underlying soil undergoes consolidation due to the gravitational load of the overburden and the gradual dissipation of pore water overpressure  $p(x, z, t)$ . Here, a 2-D groundwater flow model coupled to a 1-D geomechanical module of a compacting/accreting marsh soil is implemented to simulate the consolidation process under the hypothesis large soil deformations (Zoccarato & Teatini, 2017). Indeed, because of their typical large porosity, and consequently compressibility, shallow soils characterizing coastal wetlands experience significant compaction, possibly up to 50% in the case of decameter-thick deposits (van Asselen, 2011; Zoccarato et al., 2018). Consequently, the hypothesis of infinitesimal deformations must be released.

The flow and the displacement fields are computed through a one-way coupling approach through the following main steps. First, the deposition thickness  $\omega(x, t) \cdot \Delta t$  above the marsh platform over the time interval  $\Delta t$  is computed according to the outcome of the biomorphological model (equation (4)). Then, the total stress,  $\sigma_t$ , is updated accounting for the total weight of the soil burden, which causes overpressure within the marsh. The governing equation of the groundwater flow accounting for sediment deposition reads (Zoccarato & Teatini, 2017)

$$\frac{\partial}{\partial x} \left( \frac{k_x}{\gamma} \frac{\partial p}{\partial x} \right) + \frac{\partial}{\partial z} \left( \frac{k_z}{\gamma} \frac{\partial p}{\partial z} \right) = (c_b + \phi \beta) Dp - 2\beta k_z \frac{\partial p}{\partial z} - \beta \frac{k_x}{\gamma} \left( \frac{\partial p}{\partial x} \right)^2 - \beta \frac{k_z}{\gamma} \left( \frac{\partial p}{\partial z} \right)^2 - c_b D\sigma_t \quad (9)$$

and it is solved in a 2-D domain (Figure 1b) by using a Lagrangian approach where the Eulerian derivative  $Dp$  can be treated as a partial time derivative  $\partial p / \partial t$ . In equation (9),  $k_x$  and  $k_z$  are the horizontal and vertical hydraulic conductivities,  $\gamma$  is the specific weight of water,  $c_b$  is the soil oedometric compressibility,  $\phi$  is the soil matrix porosity,  $\beta$  is the volumetric water compressibility, and  $p$  is the incremental pore pressure with reference to the hydrostatic condition (overpressure). The variation of the total stress,  $D\sigma_t$ , is due to the load change caused by new sediments deposition over the surface, thus  $D\sigma_t = \omega(x, t)(1 - \phi_0)(\gamma_s - \gamma)$ . Once the overpressure is computed,  $\Delta z_t(x, t)$  is determined as

$$\Delta z_t(x, t) = - \int_0^{z_t} \frac{\alpha \sigma_z}{1 - \alpha \sigma_z} dz, \quad (10)$$

where  $\alpha$  is the classical vertical soil compressibility and  $\sigma_z$  is the intergranular effective stress computed according to the Terzaghi's principle,  $\sigma_z = \sigma_t - p$ . The numerical solution of equations 9 and 10 is performed by using a Lagrangian approach (Gambolati et al., 1998), where a finite element (FE)-adaptive mesh is employed with the grid nodes following the grains in their consolidation movements. The element number increases in time to account for the deposition of new material on the marsh surface. An iterative scheme is implemented to solve the two equations because of the nonlinearities arising from the dependence of the hydro-geomechanical properties on  $\sigma_z$ , that is,  $k_x$ ,  $k_z$ ,  $\phi$ ,  $\alpha$ , and  $c_b$  are functions of  $\sigma_z$ . Notice that  $\sigma_z = \sigma_z(x, z, t)$ . The compressibility  $\alpha$  is defined as  $\delta(\Delta z_t) / (\Delta z_t \Delta \sigma_z)$ . The oedometric compressibility is obtained from laboratory tests and it can be expressed as

$$c_b = - \frac{1}{1 + e} \cdot \frac{de}{d\sigma_z}, \quad (11)$$

with  $e = \frac{\phi}{(1-\phi)}$  the void ratio. The relationship between  $\alpha$  and  $c_b$  can be easily derived and reads (Gambolati et al., 1998)

$$c_b = \frac{\sigma_z \frac{d\alpha}{d\sigma_z} + \alpha}{1 - \alpha \sigma_z}. \quad (12)$$

Finally,  $\gamma = 1035 \text{ kg/m}^3$  and  $\beta = 4.32 \times 10^{-9} \text{ m}^2/\text{kg}$  are used.

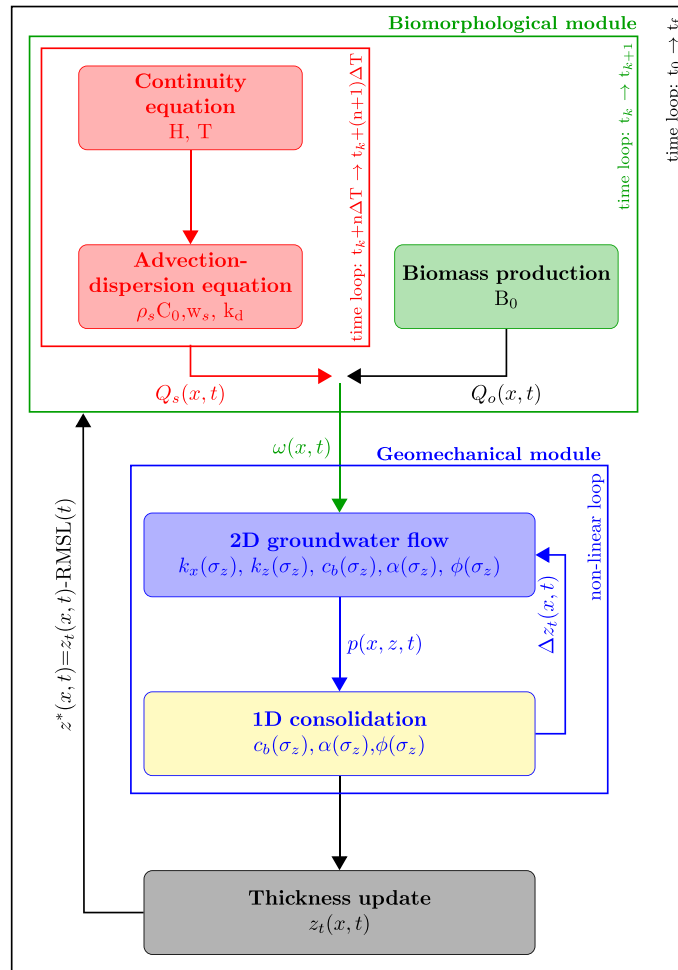


**Figure 3.** Biomorpho-geomechanical model: workflow of the staggered coupling approach implemented between the biomorphological and geomechanical modules. The dependencies on the model parameters and the temporal scales of the simulated processes are highlighted.

### 2.3. Biomorphological-Geomechanical Coupling

As mentioned above, the geomechanical model describes the long-term evolution of  $z_t(x, t)$  following the overpressure dissipation  $p(x, z)$  along a vertical transect of the landform. The forcing term of the model is represented by the deposition rate  $\omega(x, t)$  on the marsh surface, acting as a load for the underlying sediments. The deposition rates, which depend on (i) the relative elevation of the marsh surface with respect to the water level, (ii) the biomass production by vegetation decomposition, (iii) the typical tidal cycle, and (iv) the SSC in the tidal channel, are provided by the outcome of the biomorphological model. The external stressor is represented by the RSLR.

Figure 3 shows the workflow of the modeling procedure and the parameter dependencies of the biomorphological and hydro-geomechanical modules. The average sedimentation rate is first computed by the biomorphological module and then used as input to run the consolidation module that, in turn, iteratively solves the 2-D groundwater flow equation and the 1D geomechanical equation. Once the convergence of the nonlinear system is achieved, the FE grid is updated by deforming the elements and/or adding the necessary nodes. This implies the general modification of  $z_t(x, t)$  and the update of  $z^*(x, t)$  (equation (2)). Then,  $z^*(x, t)$  is used as input in the biomorphological model at the next time step to compute the new values of  $\omega(x, t)$ .

The model takes into account the effect of sea-level rise and deep subsidence (e.g., due to regional tectonics) by appropriately updating the relative position of the msl and the marsh basement. This contribution generally increases the water depth over the tidal marsh and, consequently, the deposition capacity of the system. Marsh compaction also contributes to enhance water depth by reducing  $z_t(x, t)$ .

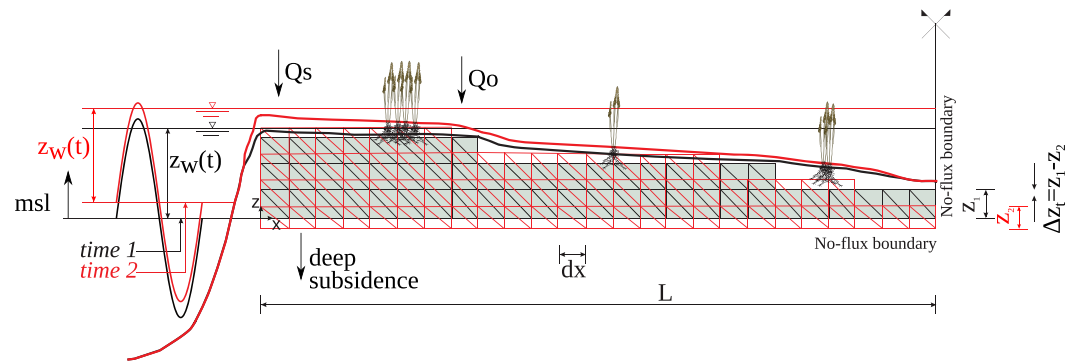


**Figure 4.** Schematic representation of the tidal marsh evolution over the time interval between  $t_1$  (in black) and  $t_2$  (in red). Inorganic and organic deposition contributes to the surface accretion with respect to RSLR, which accounts for sea-level rise and deep subsidence. The shallow compaction  $\Delta z_i$  is highlighted by the reduced thickness  $z_2$  of the finite element FEs at  $t_2$  with respect to  $z_1$  at  $t_1$ .

Different temporal scales (Figures 2 and 3) are considered in this model to properly follow the characteristic timescale of each process. Coupling multiple temporal scales is a typical challenging issue in numerical modeling. For example, a well-known case deals with surface and subsurface water flow. In the CATHY (CATchment HYdrology) simulator, Camporese et al. (2010) developed a nested time-stepping procedure to effectively couple the faster (surface) and slower (subsurface) water movements. In biomorphological models, coupling of bottom profile changes occurring over the period typical of the morphological scale (one to several years) with biotic and abiotic processes solved at the smaller timescale of a single tidal cycle (Da Lio et al., 2013) is needed. Among available strategies to couple these processes (Roelvink, 2006), we use the concept of “morphological scale factor” introduced by Lesser et al. (2004) within the Delft3D simulator and later applied in Zhang et al. (2016) to couple hydrological and morphological state variables that evolve over different timescales. The advection-diffusion equation is solved at the flow scale and the bottom changes over a tidal cycle are multiplied by a constant “scale factor” to obtain the bottom dynamics over the morphological timescale. In the modeling approach here presented, the coupling of biomorphological and geomechanical modules is treated as follows:

- over the inner time loop (Figure 3; red section), equations 6 and 7 are solved with time step  $\Delta\tau$ , which is in the order of a minute, to compute the SSC changes within the tidal cycle  $\Delta T$ , that is, 12 hr by using a semidiurnal tidal cycle;
- the deposition rate  $\omega$  is obtained by employing equations 4, 5, and equation (8) from time  $t_k$  to  $t_{k+1}$  (Figure 3; green section), with time step  $\Delta t$  on the order of a few years and
- the output  $\omega$  from the previous step is used as input into the geomechanical model (Figure 3; blue section), where the nonlinear loop is solved at every time step  $\Delta t$ . The marsh thickness is updated and used at the next step within the biomorphological module.

The  $\Delta\tau$ ,  $\Delta T$ , and  $\Delta t$  values are chosen according to temporal scales used in Marani et al. (2010) and Zoccarato and Teatini (2017). The steps are repetitively solved to simulate the marsh evolution over the long-term scale (thousands of years) from  $t_0$  to  $t_f$ , that is, the initial and final simulation times.

### 3. Reference Case

#### 3.1. Model Set-up

Figure 4 sketches the initial configuration of the tidal marsh at time  $t_1$  and a general evolution at time  $t_2$ . The modelled marsh transect is 30 m-long, representing half the distance between two tidal creeks (the right edge is a symmetry axis). This is the typical dimension of tidal marshes in the Venice Lagoon, Italy, where marsh extent ranges between 20 to and 100 m (Silvestri et al., 2005). Above a 0.05 m-thick basement, representing the top of the older (e.g., Pleistocene) alluvial stiff deposits, a structured mesh develops over time simulating the tidal marsh aggradation due to the sediment deposition. A horizontal spatial discretization  $\Delta x=0.05$  m is used and a new grid node adds up to the mesh at each  $x$ -location when the accumulated material over the surface exceeds a threshold thickness of 0.05 m. Simultaneously, the porous medium undergoes consolidation due to the overlaying soil burden and the elements constituting the FE mesh deform accordingly.

**Table 1**  
*Biomorphological and Hydro-Geomechanical Parameters Used to Simulate the Reference Case*

Biomorphological parameters		
Grain density	$\rho_s$	2650 kg/m <sup>3</sup>
SSC in the channel	$C_0$	20 mg/l
Settling velocity	$w_s$	10 <sup>-4</sup> m/s
Dispersion coefficient	$k_d$	1.5 m <sup>2</sup> /s
Maximum biomass density	$B_0$	1.0 kg/m <sup>2</sup>
Vegetation coefficient	$\gamma_b$	2.5 · 10 <sup>-3</sup> m <sup>3</sup> /yr/kg
Maximum tidal amplitude	$H$	0.5 m
Tidal period	$\Delta T$	12 hours
Hydro-geomechanical parameters		
Vertical permeability	$k_z$	10 <sup>-7</sup> m/s
Horizontal permeability	$k_x$	2.0 · 10 <sup>-7</sup> m/s
Compression coefficient	$C_c$	0.7
Surficial porosity	$\phi_0$	0.75
Surficial void ratio	$e_0$	3.00

The biomorphological model is solved by imposing the following boundary conditions. Constant concentration is set at  $x = 0$  (i.e.,  $C(0, t) = C_0$ ), no-flux concentration condition at  $x = L$  (i.e.,  $\frac{\partial C}{\partial x} \Big|_{x=L} = 0$ ) in Equation (6), and a null fluid advective velocity at  $x = L$  (i.e.,  $u = 0|_{x=L}$ ) in Equation (7). In the hydro-geomechanical model the basement is assumed impermeable (i.e.,  $\frac{\partial p}{\partial z} \Big|_{z=0} = 0$ ). Dirichlet's conditions with null values, i.e., hydrostatic pressure, are imposed on the nodes in contact with the tidal channel (i.e.,  $p(0, z, t) = 0$ ) and on the marsh surface (i.e.,  $p(0, z_r, t) = 0$ ). The right edge of the domain is a no-flux boundary representing a symmetry axis for the marsh (i.e.,  $\frac{\partial p}{\partial x} \Big|_{x=L} = 0$ ).

A reference test case is run using the model parameters reported in Table 1. The SSC in the tidal channel,  $C_0$ , is assumed constant over the tidal cycles (Carniello et al., 2014),  $w_s$  is estimated on the basis of a typical sandy-silt 20  $\mu\text{m}$  sediment size (Gibbs, 1985), and  $k_d$  is based on the work by Elder (1959). The biomass coefficients  $\gamma_b$  and  $B_0$  are taken from Marani et al. (2010) and Mudd et al. (2009). The values of the vertical and horizontal permeability are derived after Brain et al. (2011) and are assumed independent of  $\sigma_z$ . Concerning the relationships  $c_b(\sigma_z)$ ,  $\alpha(\sigma_z)$ , and  $\phi(\sigma_z)$ , they are obtained by quantifying the initial void ratio,  $e_0$ , and the compression index,  $C_c$ , from oedometric laboratory tests and then using the relationship  $e - \sigma_z$ :

$$e = e_0 - C_c \log_{10} \sigma_z \quad (13)$$

and  $c_b - \sigma_z$ :

$$-\frac{1}{1+e} \cdot de = c_b \cdot d\sigma_z \quad (14)$$

The relationship  $\alpha - \sigma_z$  derives from Equation (12). For the sake of simplicity, inorganic and organic soils are here characterized by the same properties, see Table 1.

The RSLR is assumed constant over the simulation and equal to 2 mm/yr (Carbognin et al., 2010). The long-term simulation of the tidal marsh evolution spans a time interval equal to 1,000 years with a discretization time step  $\Delta t = 0.5$  years. Thus, the organic and inorganic depositions  $Q_s$  and  $Q_o$  are average values over  $\Delta t$ , corresponding to the coupling interval between the biomorphological and geomechanical modules. Within the biomorphological model, the discretization interval  $\Delta \tau$  is used to solve Equations 6 and 7 over the tidal period  $\Delta T$  is 30 s.

### 3.2. Results

Figure 5a shows the time evolution of the tidal marsh thickness  $z_t$  as computed by the model. The  $z_t$  value increases with time providing a variable topography that depends on the distance from the tidal channel, with a difference of about 0.25 m between the left and right edges of the marsh at  $t = 1,000$  year. Note that

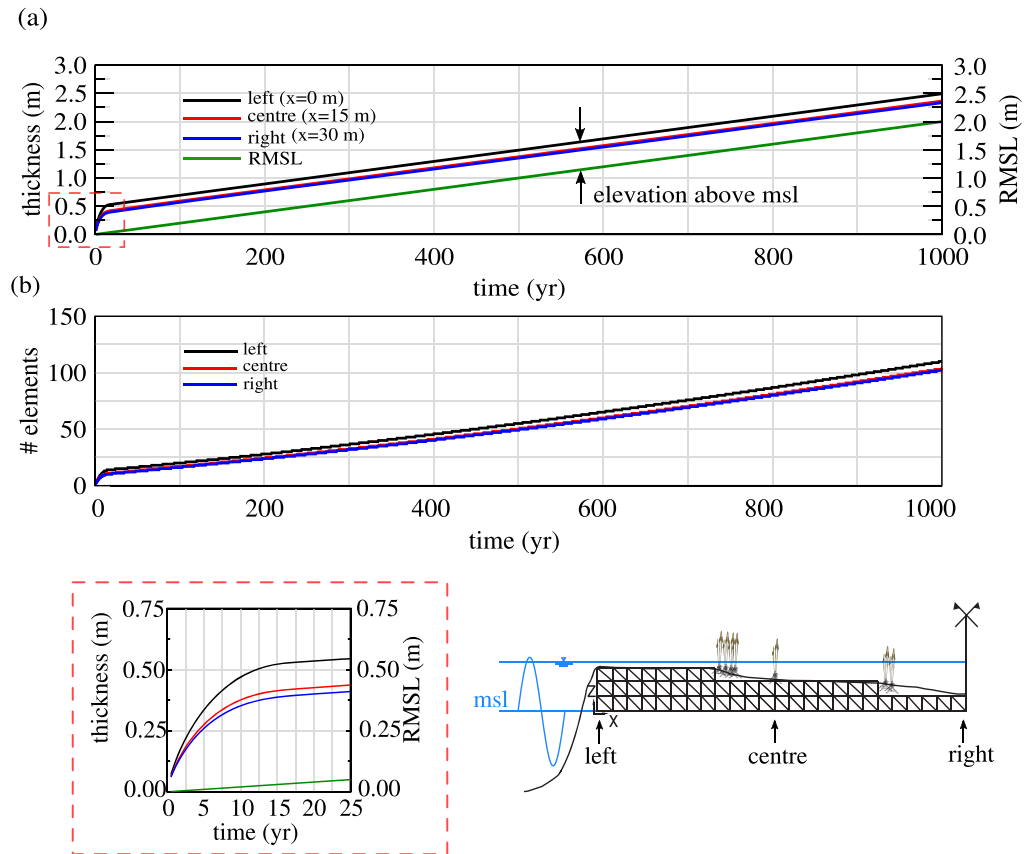


**Figure 5.** Time evolution over 1,000 years of (a) tidal marsh thickness and RMSL and (b) number of mesh elements at three locations shown in the bottom-right inset. The bottom-left zoom shows the non-linear transitional phase (25–30 years) of the marsh thickness from Sub-panel (a).

this difference increases in time. In the same figure, the RMSL is also provided. By using this set of parameters (Table 1), the tidal marsh surface is always higher than the msl, with elevation  $z^* \approx 0.50$  m (left edge) and  $z^* \approx 0.27$  m (center and right edges) at  $t = 1,000$  year. This difference is mainly due to a SSC decrease as the distance from the tidal channel increases. Figure 5b shows how the number of FEs grows at three representative locations. Notice that a number of 100 elements, each of them initially 0.05 m thick, and  $z_t \approx 2.5$  m at  $t = 1,000$  year imply that the deposited sediments compacted by approximately 50% during the period of the marsh formation.

Excluding an initial  $\sim 20$ -year highly non-linear transitional phase, the processes of deposition/compaction yield a thickness increase almost linear in time, indicating an equilibrium of the tidal marsh elevation with respect to the RMSL. In fact, as the msl rises and/or the marsh bottom deepens, the water depth over the marsh increases and a higher deposition potentially takes place yielding, however, a larger compaction. The balance between RSLR, sedimentation, and compaction develops with a water depth equal to 0.5 m at the marsh margin. Differently, the inner part of the marsh gently but continuously loses elevation relative to the msl, meaning that the sedimentation cannot balance the ongoing compaction plus RSLR.

It is also interesting to analyze how each process contributes to the total thickness  $z_t(x, t)$ . Figure 6 shows the cumulative values of inorganic and organic depositions, compaction, and RMSL along the marsh transect at  $t = 1$  year (Figure 6a),  $t = 500$  years (Figure 6b), and  $t = 1,000$  years (Figure 6c). At the onset of the simulation (Figure 6a), the major accretion supply is due to mineral deposition with  $Q_s = 0.089$  m at  $x = 0$  m. Net accretion by organic matter is 5% of total deposition. On the other hand, shortening caused by consolidation amounts to  $\Delta z_t = -0.004$  m and  $\text{RMSL} = 0.001$  m.  $Q_s$  values generally decrease for  $x > 0$  m, whereas  $Q_o$ ,  $\Delta z$ , and RMSL are substantially constant along the marsh transect. At  $t = 500$  years, Figure 6b shows a contribution by  $Q_s$  up to 2.70 m at  $x = 0$  m.  $Q_o$  almost vanishes at  $x = 0$  m but increases with  $x$ , reaching the maximum value  $Q_o = 0.44$  m at  $x = L$ . Indeed, the biomass production is higher at lower

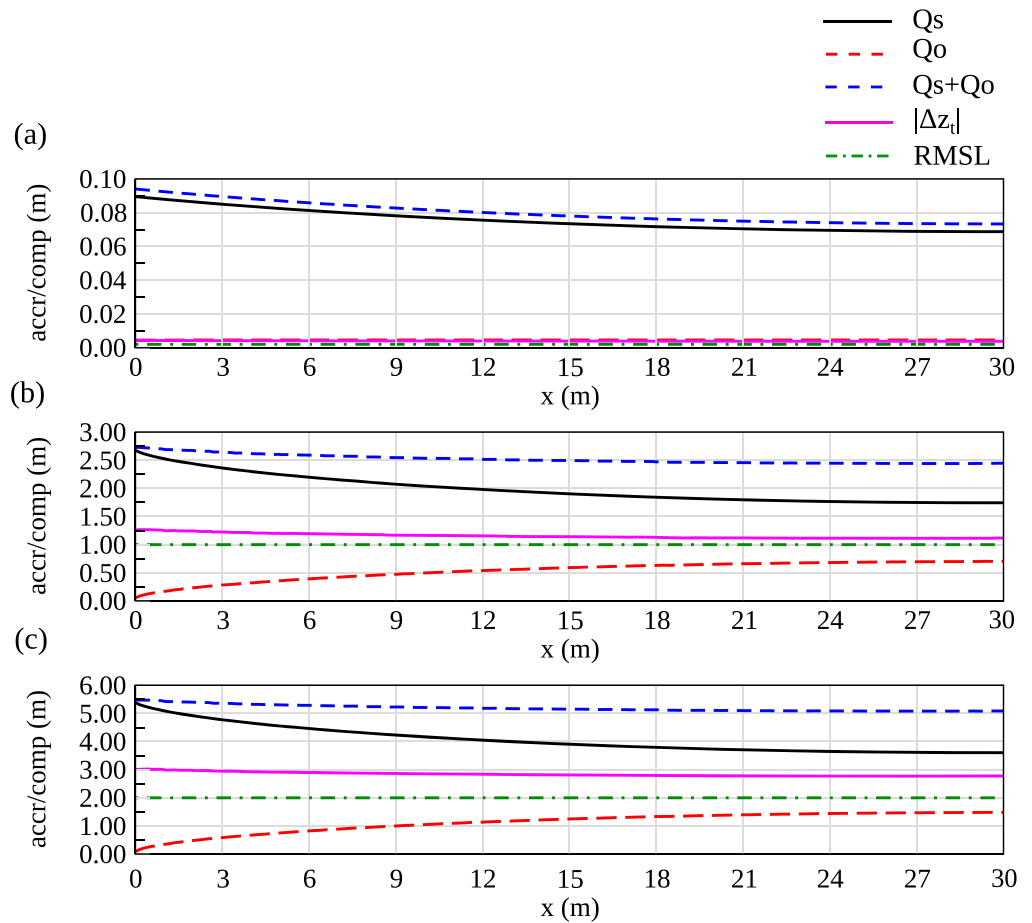


**Figure 6.** Spatial distribution of the processes responsible for the marsh thickness at time (a)  $t = 1$  year, (b)  $t = 500$  years, and (c)  $t = 1,000$  years: cumulative values of inorganic and organic accretion ( $Q_s$  and  $Q_o$ ), compaction ( $\Delta z_t$ ), and RMSL. Note the different y-axis scale in the sub-panels where accretion and compaction are plotted.

elevations following Equation (8).  $\Delta z_t$  and RMSL amount to similar values in the range 1.0–1.25 m. The behaviors at  $t = 1,000$  years (Figure 6c) mostly resemble the previous one with the exception of  $\Delta z_t$  that non-linearly increases with time. To give an example, the thickness  $z_t(0, 1000) = 2.47$  m, that is, at the tidal creek and at the end of the simulation, (Figure 5a, black line) is contributed by  $Q_s + Q_o + \Delta z_t = 5.42\text{ m} + 0.048\text{ m} - 3.00\text{ m}$ . The elevation above msl  $z^*(0, 1000)$  is then obtained by  $z_t(0, 1000) - \text{RMSL} = 2.47\text{ m} - 2.00\text{ m} = 0.47\text{ m}$  (highlighted by the arrows in Figure 5a).

## 4. Model Sensitivity

### 4.1. Investigating the Contribution of the Various Processes

In this section, the values of the parameters used in the reference case are varied to stress the role exerted by each of the processes addressed by the coupled model. The analyses focus on the geomechanical parameters  $C_c$  and  $\phi_0$  (Case A), the SSC in the tidal channel  $C_0$  (Case B), the RSLR (Case C), and the contribution of the vegetation through  $B_0$  (Case D). Table 2 summarizes the parameter values used in the sensitivity analysis.

The model results are presented in Figure 7 where the cumulative values of  $Q_s$ ,  $Q_o$ , and  $\Delta z_t$  computed for the four test Cases A to D are compared with the reference case at  $t = 1,000$  year for (a)  $x = 0$  m (a) and (b)  $x = L$  (b). Note that each contribution has been normalized over the quantity  $F_{TOT} = |Q_s| + |Q_o| + |\Delta z_t|$ .

$Q_s$  is generally the largest contribution. In Figure 7a,  $Q_o$  is significantly lower than  $Q_s$ , except for Case B (low SSC in the channel) where  $Q_o$  amounts to 27%  $F_{TOT}$ . On the other hand,  $\Delta z_t$  is almost 40%  $F_{TOT}$  for all cases except when low-compressibility soil and, secondarily, low RSLR are accounted for (Figure 7a, Cases A and C). Interestingly,  $Q_s$  peaks the highest percentage ( $Q_s = 91\%F_{TOT}$ ) in Case A with a low-compressibility

**Table 2**  
Test Cases A-D Used to Analyze the Influence of the Forcing Parameters on the Model Outcome

Test case	Parameters	Reference Case	#1 (low)	#2 (high)	References
A	$C_c ; \phi_0$	0.7; 0.75	0.024; 0.52	1.2; 0.79	Brain et al. (2011) Brain et al. (2017)
B	$C_0$ (mg/l)	20	1	40	Carniello et al. (2014)
C	RSLR (mm/yr)	2	0	10	Tosi et al. (2009) Church et al. (2013) Jankowski et al. (2017)
D	$B_0$ (kg/m <sup>2</sup> )	1	0	2	Morris and Haskin (1990) Scarton et al. (1998)

Note. The values represent admissible bounds provided by literature.

soil (Figure 7a). Also, notice in Figure 7a (Case C) that the  $Q_s$  percentage decreases with RSLR and, conversely,  $\Delta z_t$  increases.

Differently, Figure 7b shows that a considerable organic contribution usually occurs at  $x = L$ . The largest percentage is computed in Case A ( $Q_o = 42\% F_{TOT}$ ). In Case B, low  $C_0$ ,  $Q_o = 38\%$  is even larger than  $Q_s = 25\% F_{TOT}$ . Also, in the reference case and with high  $C_0$ ,  $Q_o$  contributes significantly (19% and 27%, respectively) to  $F_{TOT}$ . The contribution of the organic matter is greater at  $x = L$  than at  $x = 0$  m due to the fitness function shape adopted in the model (Equation (8)). Finally, notice that the lack of organic soil deposition (Case D) provides an increase of the  $Q_s$  percentage relative to the reference case larger at  $x = L$  than at the tidal creek. Indeed,  $Q_o = 0$  leaves more “space” free to sedimentation of inorganic deposits in the inner part of the marsh than at  $x = 0$  m. Conversely,  $\Delta z_t$  keeps a similar percentage contribution along the whole transect because of the simplifying assumption that the inorganic and organic soils are characterized by the same geomechanical properties. A more specific analysis should take into account that organic soils are more compressible but lighter than inorganic deposits.

#### 4.2. Investigating the Importance of Shallow Compaction

The relative importance of compaction and aggradation on the evolution of a tidal marsh with respect to RSLR has been highlighted in the previous section by means of Cases A and C. Here, it is investigated in more detail how the tidal marsh resilience can vary under different compaction and RSLR values. The results are

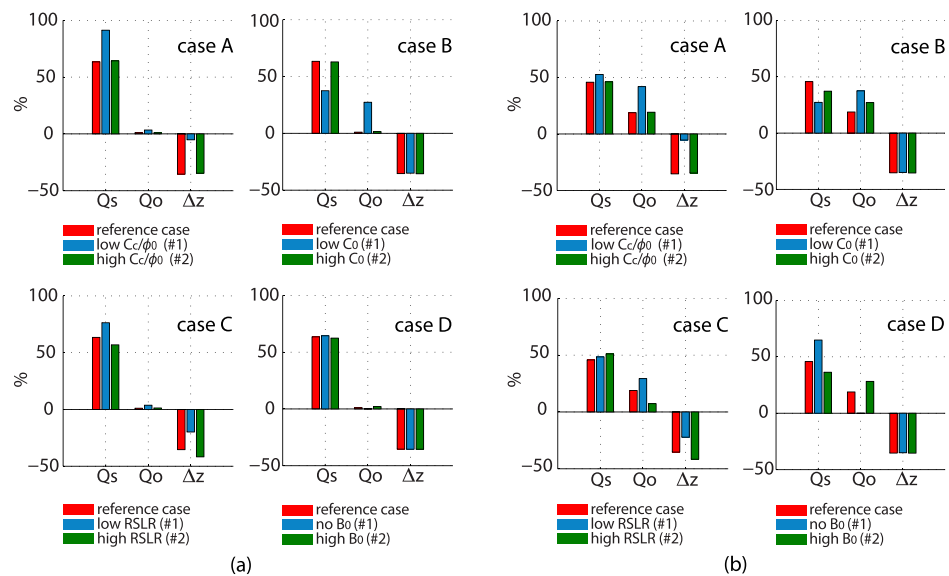


**Figure 7.** Contribution (%) of  $Q_s$ ,  $Q_o$ ,  $\Delta z_t$  in shaping the tidal marsh thickness at (a)  $x = 0$  m (a) and (b)  $x = L$  (b). The roles of sediment compressibility (Case A), suspended-sediment concentration SSC in the tidal channel (Case B), relative sea-level rise RSLR (Case C), and organic matter production (Case D) are investigated.

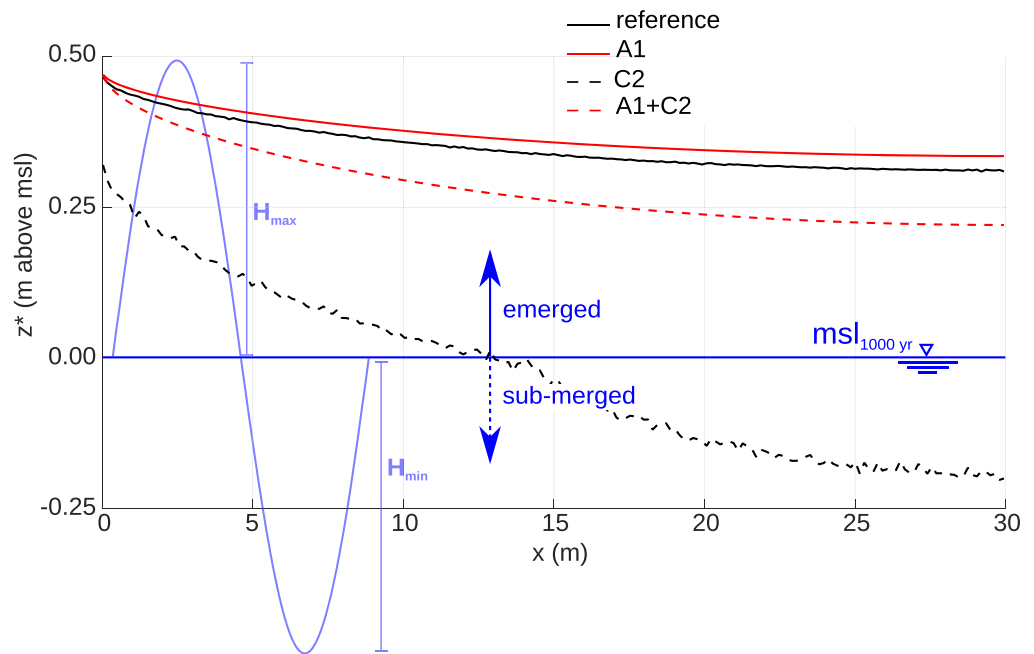


**Figure 8.** Tidal marsh elevation above msl at time  $t = 1,000$  year. Different topographies are obtained by varying the geomechanical properties and/or the relative sea-level rise (RSLR) according to the scenarios defined in Table 2. The tidal marsh undergoes partial submersion on the inner portion of the transect if the marsh is constituted by organic silty soil and RSLR = 10 mm/yr.

presented in Figure 8 in terms of  $z^*$  along the marsh transect at  $t = 1,000$  years. The reference case, where the marsh is made of organic silty soil (Table 1), is compared to the cases where: (i) the shallow compaction is negligible because the marsh is composed of sandy loam (Case A1, Table 2), (ii) the RSLR amounts to 10 mm/yr (Case C2, Table 2), and (iii) the combination A1 plus C2.

As long as the RSLR is relatively small, the marsh elevation results almost independent on the soil properties: the profiles shown in Figure 8 for the reference and the A1 cases differ of a few centimeters only, with the marsh surface that remains well above the actual msl. Conversely, when a high RSLR value is taken into account, the soil compressibility and porosity play a major role: if the marsh is still able to follow the RSLR when the soil is relatively stiff (Case A1 + C2), more than half of the inner part becomes submerged when a more compressible organic soil is supposed to compose the landform (Case C2). Only the part closer to the tidal creek remains above msl in this scenario.

Figure 9, which shows the temporal behavior of  $Q_s$ ,  $Q_o$ , and  $\Delta z_t$  at the two boundaries of the transect for the four investigated test cases, helps in understanding how the various biogeomorphological processes combine to provide the elevation profiles summarized in Figure 8. For all the profiles, the computed values are meaningful after the first  $\sim 20$ -yr non-linear transitional phase (Figure 5). Figure 8 shows that, when RSLR is relatively small, the marsh elevation above the actual msl is almost independent on soil compressibility. Inspection of Figures 9a and 9e reveals that  $Q_s$  and  $\Delta z_t$  assume very different values in the two cases but they sum up to a similar amount. If soil compacts more because the compressibility is larger,  $H - z^*$ , that is, the water depth above the tidal marsh, is larger and favours a greater deposition. Therefore, from the point of view of the marsh elevation relative to the (same) msl, that is, of the marsh resilience to RSLR, the combined effects of sedimentation and compaction appears almost independent on soil compressibility. However, the processes strongly differ in the two cases: at the tidal creek, the cumulative sedimentation and compaction over the simulated 1,000 years amount to  $\sim 4.8$  m and  $\sim 2.8$  m, and to  $\sim 2$  m and  $\sim 2 \times 10^{-3}$  m with organic silty and silty loam sediments, respectively. The biomass production contributes with  $\sim 5\text{--}6 \times 10^{-2}$  m in both the cases (Figure 9c). Similarly, at  $x = L$ , the cumulative compaction does not change respect to the values at  $x = 0$  (Figure 9d), with the sedimentation contributed by inorganic deposition and biomass production that amount to  $\sim 1.0$  m and  $\sim 1.0$  m for the stiff soil scenario and to  $\sim 3.3$  m and  $\sim 1.5$  m for the compressible soil, respectively (Figures 9b and 9f).

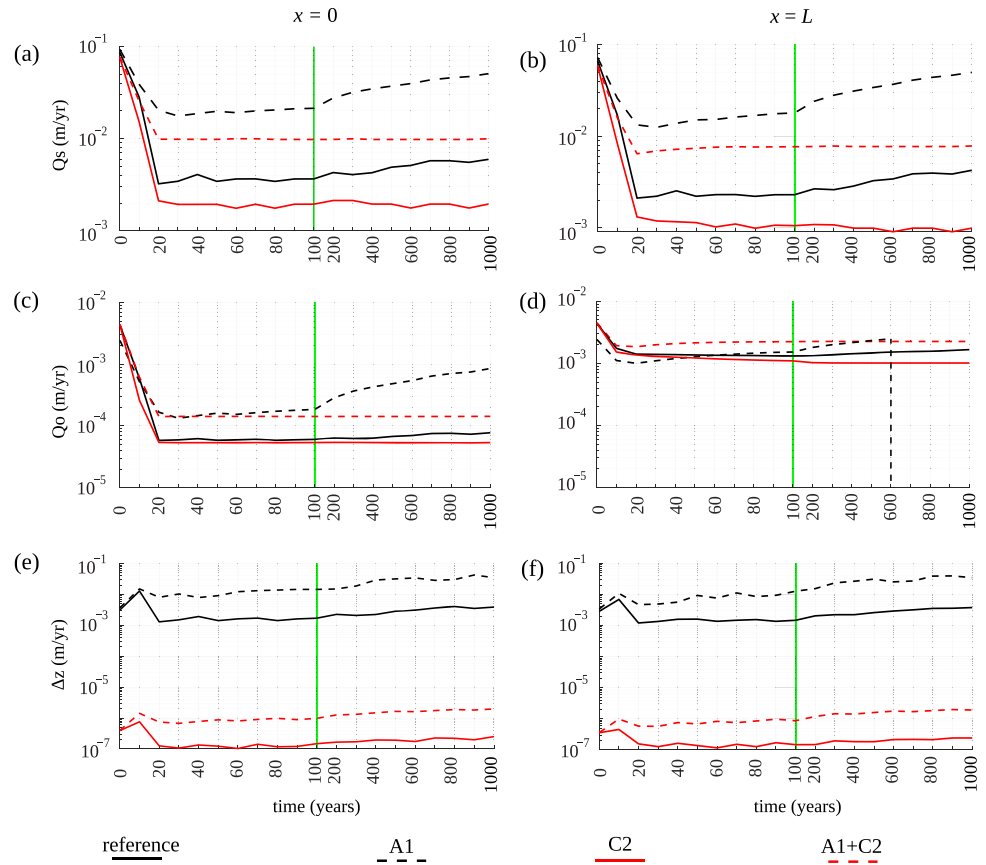


**Figure 9.**  $Q_s$ ,  $Q_0$ ,  $\Delta z$  over time at the left, that is,  $x = 0$  m (a, c, e), and right, that is,  $x = L$  (b, d, f), boundaries of the tidal marsh for the test cases presented in Figure 8. Note the different logarithmic scale on the y-axis. The green dashed lines highlight a change from decades to centuries in the x-axis scale.

Similar considerations on the relative contribution of  $Q_s$ ,  $Q_0$ , and  $\Delta z_t$  hold with RSLR = 10 mm/yr (case C2 and case A1+C2). Certainly, the sedimentation and compaction amounts are much larger in these cases, with the final marsh thickness averaging 10 m. Interestingly, Figure 9d reveals that if a more compressible organic silt composes the marsh, the biomass production nulls ( $Q_0$ ) at  $t \sim 600$  years, meaning that the surface of the tidal marsh becomes lower than the actual msl at that time. Therefore, the inner part of the marsh becomes an unvegetated pond. Comparison of Figures 8 and 9d reveals that, with conditions accounted for in Case C2, the pond radius enlarges about 17 m over the last 400 years encompassed by the simulation. Lack of organic soil aggradation, reduced sedimentation of inorganic deposits because of the distance from the tidal creek, and ongoing compaction of the marsh body contribute to the ponding enlargement.

### 5. A Realistic Test Case

The proposed coupled model is finally tested on a realistic case. The evolution of a tidal marsh in the Venice Lagoon is investigated from the beginning of its formation until present, and then to 2100 AD (anno Domini) for two scenarios of RSLR and lagoon management. The application does not claim to provide a picture of a specific marsh but rather must be viewed as a preliminary application using average information from the central basin of the Venice Lagoon.

The simulation spans 6,600 years, that is, from 6500 yr before present (BP) to 2100 AD. For the sake of simplicity, the “present date,” that is,  $t = 0$  years BP corresponds to the year 2000 AD. The Lagoon of Venice originated nearly 6-7 kyr BP during the Holocene transgression, when the rising sea flooded the North Adriatic Pleistocene plain and outlined the coast in approximately the present position (Brambati et al., 2003). The simulation has been carried out using the reference case data set. Indeed, both the biomorphological

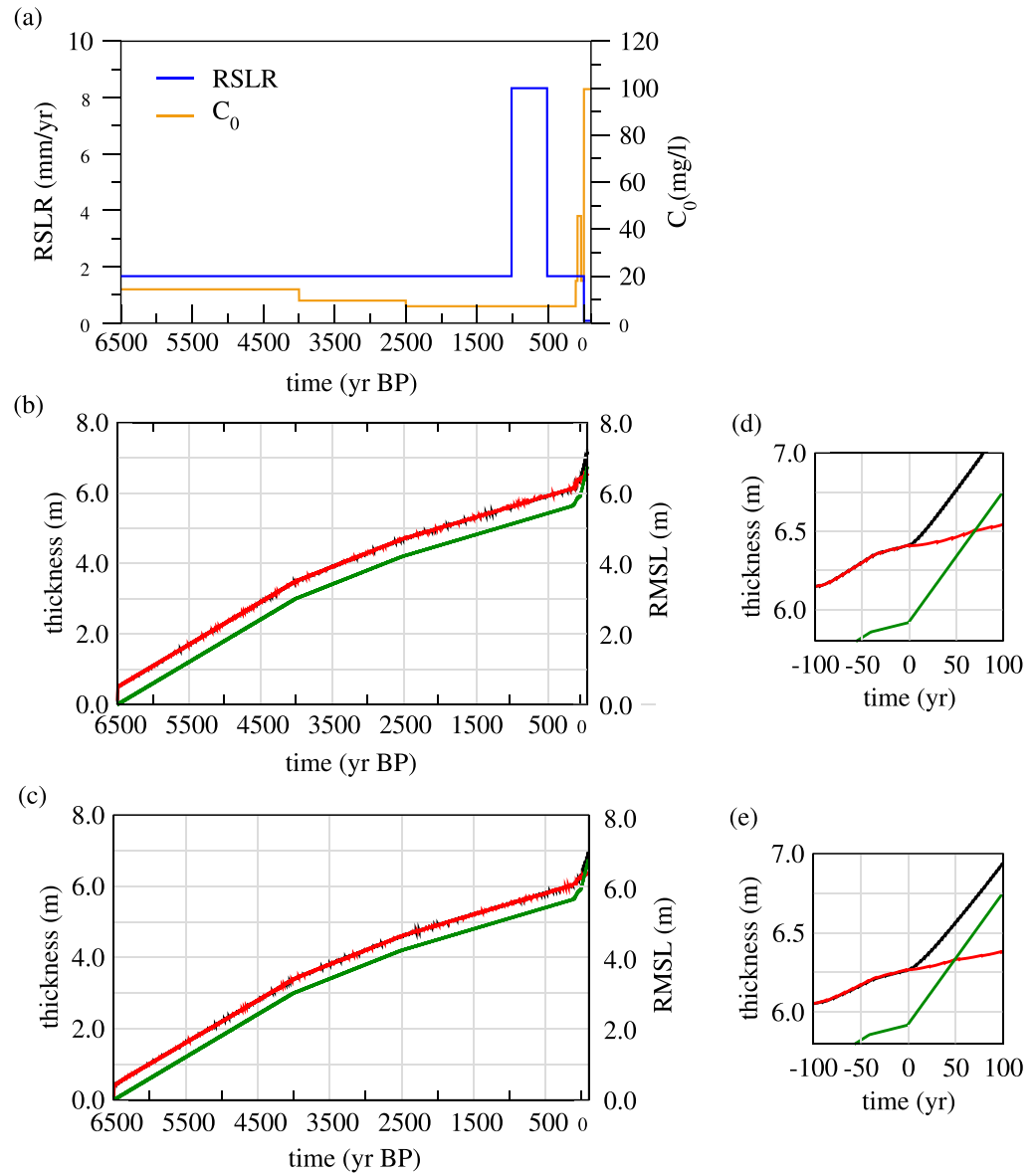


**Figure 10.** (a) Relative sea-level rise (RSLR) and  $C_0$  versus time as assumed in the realistic scenarios spanning the period between 6500 and 0 yr BP plus a 100-year future projection (a). Time behavior of the tidal marsh thickness (b)  $z_t$  at  $x = 0$  m (b) and (c)  $x = L$  (c) under the hypotheses of a time-dependent RSLR only (black profile) or a simultaneous variability over time of RSLR and  $C_0$  (red profile). The RMSL is shown in green. A zoom of the model outcomes from 0 yr BP to 2100 is provided in (d) and (e) for  $x = 0$  m and  $x = L$ , respectively.

and the hydro-geomechanical parameters provided in Table 1 can be assumed representative of the typical setting in the Venice Lagoon (Cola et al., 2008; Da Lio et al., 2013; Silvestri et al., 2005).

The simulations have been carried out substituting the constant  $RSLR = 2$  mm/yr used in the reference case with a time-dependent behavior (Figure 10a). According to Lambeck et al. (2011), the average RSLR in the Northern Adriatic Ssea amounted to 1.2 mm/yr between 4500 BC (before Christ) and 2000 BC (i.e., from 6500 to 4000 yr BP), 0.8 mm/yr between 2000 BC and 500 BC (i.e., from 4000 to 2500 yr BP), and 0.6 mm/yr between 500 BC and 1900 AD (i.e., from 2500 to 100 yr BP). Eustatic sea-level rise and tectonics contributed to these values. The records provided by tide gauge at Punta della Salute, Venice, have been used to characterize RSLR over the last decades (Carbognin et al., 2004, 2010). An average value equal to 1.5 mm/yr was measured between 1900 AD and 1920 AD (i.e., from 100 to 80 yr BP) and between 1970 AD and 2000 AD (i.e., from 30 yr BP to now). Between 1920 AD to 1970 AD (i.e., from 80 to 30 yr BP), the

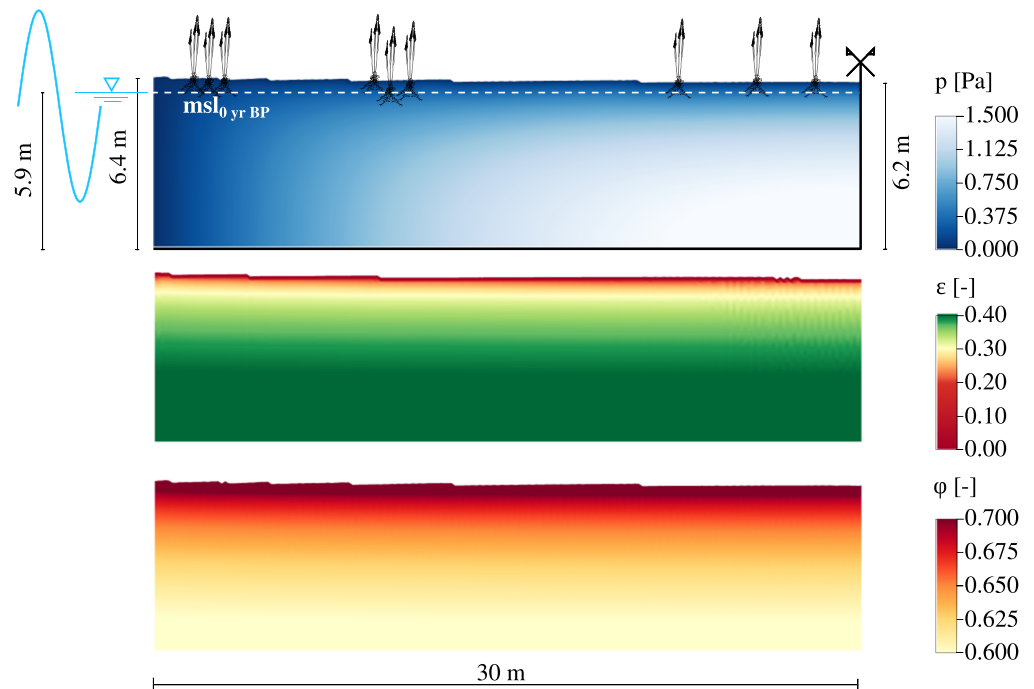


**Figure 11.** Spatial distribution of (a) pore pressure (a), (b) vertical strain (b), and (c) porosity (c) within the marsh transect at  $t=0$  years BP. At this time, the tidal marsh elevation is approximately 0.5 m and 0.3 m above the actual msl at the creek and inner boundary, respectively.

central portion of the lagoon subsided significantly because of groundwater pumping from a 100-300 m deep aquifer system (Teatini et al., 1995), with an average RSLR increase to 3.8 mm/yr. Concerning the period from 2000 AD to 2100 AD, it has been elected to use the average SLR rate by IPCC AR5 business as usual estimate, scenario RCP8.5, which amount to 7.5 mm/yr (Church et al., 2013), plus 0.8 mm/yr representing the contribution from deep subsidence (Carminati & Di Donato, 1999; Tosi et al., 2009).

SSC has been also changed over time (Figure 10a). The information on  $C_0$  is more qualitative than that on RSLR and are indirectly derived from the historical evolution of the lagoon (D'Alpaos, 2010; Gambolati & Teatini, 2013). The reference value  $C_0 = 20$  mg/l (Carniello et al., 2014) has been assumed representative over the last centuries, specifically from today back to 500 yr BP. In order to prevent the lagoon to be silted up, the Venetians diverted all the major rivers flowing into the lagoon over the sixteenth to eighteenth centuries. Indeed, between  $\sim 1000$  AD to and  $\sim 1500$  AD, the historical documents and maps report the silting up of large portions of the lagoon, with a notable mainland advancement toward Venice due to large amount of sediments transported into the lagoon by the rivers. Reclamation of lagoon wetlands are documented between  $\sim 400$  AD and  $\sim 1000$  AD. The much larger sediment availability in the past has been accounted for by fixing  $C_0 = 100$  mg/l, that is, 5 times the present value, between 1000 yr BP to and 500 yr BP, and  $C_0 = 40$  mg/l from the beginning of the simulation (6500 yr BP) to 1000 yr BP. Concerning the period from 2000 AD to 2100 AD,  $C_0 = 1.0$  mg/l has been assumed. The drastic reduction of the sediment availability over the future could be a byproduct of the MoSE (MODULO Sperimentale Elettromeccanico) mobile barriers under construction at the inlets of the lagoon to prevent high tides (Ferrarin et al., 2013).

The model results are shown in Figures 10b and 10c. The figures show the evolution of the marsh thickness at  $x = 0$  m and  $x = L$ , over the whole time interval spanned by the analysis. Two scenarios are simulated, the first where only RSLR is variable with time and  $C_0 = 20$  mg/l, and the second one characterized by both RSLR and  $C_0$  time-dependent. Different growing trends can be identified depending on the RSLR( $t$ ) values. Clearly, a constant concentration  $C_0 = 20$  mg/l suffices to counterbalance the RMSL. Interestingly, Figures 10b and 10c show that the two scenarios provide indistinguishable outcomes at the scale of the graphical representation, suggesting that values of  $C_0$  higher than the actual one did not affect the long-term evolution of the tidal marsh. The RSLR, which is the main driver of the tidal marsh thickening, governs the water depth and, consequently, the accretion process above the tidal marsh platform. The final thickness of

the marsh amounts to  $\sim 6$  m, a value which is comparable to the thickness of the Holocene deposits in the central Lagoon of Venice (Brambati et al., 2003; Zecchin et al., 2008).

Until  $t = 0$  years BP, the marsh platform is always higher than the msl, that is, thicker than RMSL. Conversely, different behaviors can be recognized over the projection period (Figures 10d and 10e). At the tidal creek, the marsh will keep pace with the RSLR if the actual SSC will be maintained: Figure 10d shows that the distance between the marsh surface and the rising (relative) msl will remain almost constant and approximately equal to  $H$ . At  $x = L$  (Figure 10e), the marsh will progressively lose its relative elevation, likely becoming lower than the msl after 2100 AD. If the simultaneous  $C_0$  reduction is accounted for, the tidal marsh fate will worsen and the projection is harmful. The marsh surface will become lower than msl in  $\sim 70$  yr (Figure 10d) and  $\sim 50$  yr (Figure 10e) at  $x = 0$  m and  $x = L$ , respectively.

Figure 11 shows the model results within the marsh transect at  $t = 0$  yr BP for the scenario with variable RSLR and  $C_0$ . The panels show the spatial distribution of overpressure, vertical strain, and porosity. The maximum overpressure is obtained at the bottom-right corner of the marsh with a value of  $\sim 1.5$  Pa (Figure 11a). The vertical strain  $\epsilon$  (Figure 11b) is computed at the grid-element size.  $\epsilon$  is computed as  $(z_{e,t_i} - z_{e,t_f})/z_{e,t_i}$ , where  $z_{e,t_i}$  and  $z_{e,t_f}$  are the element thickness at the time of deposition and  $t = 0$  years BP, respectively. A 40% strain characterizes the marsh bottom and gradually decreases moving upward, leading to an overall  $\sim 35\%$  vertical strain of deposited organic and inorganic matter. The porosity distribution (Figure 11c) is related to  $\sigma_z(x, z)$  according to Equation (13). The highest  $\phi$  occurs at the marsh top where  $\sigma_z$  is minimum. The porosity gradually decreases from top to bottom with a maximum reduction of  $\sim 15\%$  at the marsh basement, where the soil experienced the highest consolidation.

## 6. Discussion

Tidal marshes are dynamic landforms whose evolution relative to msl has attracted the attention of various branches of the biological and physical sciences, including ecohydrology, geomorphology, Holocene geology, and coastal processes. Because of their recent and fast development, the richness of organic matter, low-density, and high compressibility of the sediments, tidal marshes can provide precise and near-continuous information on the relative sea-level changes over the last few millennia (Brain et al., 2017). On the other hand, it is likewise important to understand how biotic and abiotic processes will interact with the expected sea-level rise and local human interventions to drive the marsh evolution over the next decades and centuries (Kirwan & Murray, 2007).

A link between the evolution of marshes over the Holocene and their resilience over the future appears highly probable. This connection has been recently discussed by (Horton et al., 2018), who developed a statistical procedure to assess the future limits to marsh vulnerability for Great Britain by analyzing reconstructions of tidal marsh retreat and expansion during the Holocene. Along this context, the basic concept we have investigated in this contribution is that a tidal marsh is not only a “surface” above which ecological and morphological processes take place, as intrinsically assumed by the majority of the modeling studies carried out to represent tidal marsh evolution (e.g., Fagherazzi et al., 2012). From our point of view, a tidal marsh must be considered more appropriately as a 3-D body of recently deposited sediments. Therefore, its evolution does not depend only on what happens on the surface in terms of external stressors (deposition, erosion, organic matter decomposition, relative sea-level rise), but also on the intrinsic properties of the landform itself.

The results presented in this work demonstrate the importance of a coupled surface-subsurface dynamical analysis and highlight the broad implications of our findings on the fate of coastal wetlands in response to RSLR. Previous works (Deegan et al., 2012; Kirwan & Murray, 2007; Long et al., 2006; Marani et al., 2010) have clearly pointed out how climate-related stressors exert a strong control on the tidal landform states when ecogeomorphological thresholds are exceeded. We have shown that, with available sediment-suspended concentration  $C_0$  in the range typical of natural lagoons ( $10 < C_0 < 100$  mg/l) (Carniello et al., 2014; Marani et al., 2010), a tidal marsh is capable to maintain its elevation relative to the msl independently of RSLR values if the deposits are relatively stiff, that is, the minerogenic component prevails. If not, that is, a large percentage of organic matter composes the marsh body, the landform resilience is much more dependent on RSLR. This is supported by the observation that, generally, vegetated marshes shift to unvegetated ponds and then to tidal flats starting from the inner areas (Ganju et al., 2017; Mariotti, 2016), where the percentage of organic soil is larger than in the outer parts because of the smaller elevation and

larger distance from the tidal creek. However, our explanation of pointing enlargement is different from that proposed by Mariotti (2016), who invoked the erosion of the pond banks due to waves and creep.

We are aware that the model applications here proposed are far from covering a complete sensitivity study on the effects of possible interactions between biological, morphological, hydrodynamic, and geomechanical processes in these complex transitional environments. For example, roots affect soil consolidation acting as near-surface local reinforcements that cause over-consolidation (Brain et al., 2015). The implemented geomechanical module uses as input parameter a relationship soil compressibility versus effective stress  $\sigma_z$  (Equation 11), properly accounting for a stiffer soil for  $\sigma_z$  smaller than the pre-consolidation stress. Or, marsh species are commonly observed to be maximally productive for specific range of platform elevation relative to the msl (Morris, 2006). The used biomorphological module (Da Lio et al., 2013) accounts for species zonation versus marsh topography, with biomass productivity that is linked to the percentage of organic matter in the soil, and therefore to its compressibility and compaction, through a double feedback.

Moreover, some processes playing a role on marsh platform dynamics are not yet addressed. Specifically:

- Surface erosion due to wind-induced waves (Carniello et al., 2005) is not directly included in the formulation. However, in the context of long-term simulations, it is reasonable to suppose that  $\omega$  (Equation (4)) represents the net sediment budget (sedimentation minus erosion) contributing to the annual marsh accretion.
- As stated above, sediment trapping by vegetation is neglected. According to Da Lio et al. (2013) and Mudd et al. (2010), this is a reasonable assumption in micro-tidal environments, i.e. that is, transitional areas where the tidal range is less than 2 m as the Venice Lagoon is, where the particle settling due to gravity largely dominates because of small flow velocities.

## 7. Conclusions

A novel physically-based numerical model that couples the hydro-mechanical equations controlling the evolution of a marsh thickness because of consolidation with the hydrodynamic and transport equations ruling the flow field and sediment transport above the marsh and a simplified equation of biomass production is presented. These latter provide the accretion rate on the tidal platform, that is, the shallowest uncompacted deposits thickening the marsh from the top but, simultaneously, increasing the consolidation of the underlying marsh body because of their load. The different characteristic times of the various processes are properly accounted for. The only external factor, not directly simulated by the model, is represented by the sea-level rise and the subsidence of the marsh bottom. The feedbacks between sedimentation, biomass production, consolidation, platform elevation relative to the mean sea level, and RSLR are simulated. The equations are solved on a 2-D evolving domain representing a tidal marsh transect orthogonal to a tidal channel. The model is applicable over the large temporal scales necessary for assessing the response of tidal marshes to sea-level rise, sediment supply changes, and consolidation.

Although related to simplified examples, the results obtained using realistic data sets support our understanding about the importance of coupling surface and subsurface processes to mimic the evolution of tidal marshes and predict their vulnerability and resilience in the decades to come. The major findings of general validity can be summarized as follows:

- The role of natural consolidation on the evolution of a tidal marsh surface cannot be neglected. Including this process into an external RSLR forcing term constitutes a significant approximation that can lead to erroneous interpretation of the past evolution of these transitional environments and, consequently, unreliable prediction of their evolution in the future.
- Because of high porosity and compressibility, the compaction of marsh deposits offsets a significant percentage of the surficial accretion. The value, which is dependent on the soil compressibility, can amount to more than 30%.
- Given a set of biomorphological and hydrodynamic conditions, the resilience of a marsh to a certain RSLR can be strongly affected by the geomechanical properties of the deposits composing the marsh. In particular, the (portions of) tidal marshes composed of soils rich in organic matter are more susceptible to lose elevation relative to the actual msl if RSLR is large (10 mm/yr for the specific case we simulated, but smaller values likely suffice with other parameter combinations). Otherwise, accretion and compaction

balance, independently of the soil geomechanical properties, keeping the marsh platform at an elevation above msl approximately equal to the “mean” tidal amplitude.

- The feedbacks between the surface and subsurface processes play a major role on the marsh survival. The coupled dynamics is highly nonlinear. The value of the RSLR above which a marsh starts losing elevation relative to the msl is a complex combination of the parameters governing the biogeomorphic and the geomechanical processes.

Still keeping the same 2-D model setting, the possible aspects to be further analyzed by the new coupled approach could be (i) the control played by different vegetation species in tuning marsh topography (Marani et al., 2013), (ii) the decrease of the hydraulic conductivity with the effective stress that can prolong the overpressure dissipation, and therefore, the consolidation of recently deposited coastal soils as verified by Zoccarato et al. (2018) in deltaic environments, and (iii) the dependence of soil compressibility not only on soil type and effective stress, but also on other factors, for example, the temperature at the time of deposition or the presence of undecomposed roots (Brain et al., 2017).

### Acknowledgments

This article is an outcome of the VENEZIA-2021 Research Programme, Topic 3.1, funded by the “Provveditorato Interregionale Opere Pubbliche per il Veneto, Trentino Alto Adige e Friuli Venezia Giulia” through the “Concessionario Consorzio Venezia Nuova” and coordinated by CORILA, Venice. All data used in this study are described in the article.

### References

- Adam, P. (1990). *Salt-marsh ecology*. Cambridge, UK: Cambridge University Press.
- Allen, J. R. L. (1999). Geological impact on coastal wetland landscapes: Some general effects of sediment autocompaction in the Holocene of northwest Europe. *Holocene*, 9(1), 1–12. <https://doi.org/10.1191/0959683996749296672>
- Augustin, L., Irish, J., & Lynett, P. (2009). Laboratory and numerical studies of wave damping by emergent and near-emergent wetland vegetation. *Coastal Engineering*, 56(3), 332–340.
- Blum, L. K., & Christian, R. R. (2013). Belowground production and decomposition along a tidal gradient in a Virginia salt marsh. In S. Fagherazzi, M. Marani, & L. K. Blum (Eds.), *The ecogeomorphology of tidal marshes* (pp. 47–73). Washington DC: American Geophysical Union (AGU). <https://doi.org/10.1029/CE059p0047>
- Brain, M. J., Kemp, A. C., Hawkes, A. D., Engelhart, S. E., Vane, C. H., Cahill, N., et al. (2017). Exploring mechanisms of compaction in salt-marsh sediments using Common Era relative sea-level reconstructions. *Quaternary Science Reviews*, 167(1-4), 96–111. <https://doi.org/10.1016/j.sedgeo.2010.10.005>
- Brain, M. J., Kemp, A. C., Horton, B. P., Culver, S. J., Parnell, A. C., & Cahill, N. (2015). Quantifying the contribution of sediment compaction to late Holocene salt-marsh sea-level reconstruction, North-Carolina, USA. *Quaternary Research*, 83(1), 1151. <https://doi.org/10.1016/j.yqres.2014.08.003>
- Brain, M. J., Long, A. J., Petley, D. N., Horton, B. P., & Allison, R. J. (2011). Compression behaviour of minerogenic low energy intertidal sediments. *Sedimentary Geology*, 233(1-4), 28–41. <https://doi.org/10.1016/j.sedgeo.2010.10.005>
- Brain, M. J., Long, A. J., Woodroffe, S. A., Petley, D. N., Milledge, D. G., & Parnell, A. C. (2012). Modelling the effects of sediment compaction on salt marsh reconstructions of recent sea-level rises. *Earth and Planetary Science Letters*, 345–348, 180–193. <https://doi.org/10.1016/j.epsl.2012.06.045>
- Brambati, A., Carbognin, L., Quaia, T., Teatini, P., & Tosi, L. (2003). The Lagoon of Venice: Geological setting, evolution and land subsidence. *Episodes*, 26(3), 264–268.
- Cahoon, D. R., Lynch, J. C., Hensel, P., Boumans, R., Perez, B. C., Segura, B., & Day, Jr. J. W. (2002). High-precision measurements of wetland sediment elevation: I. Recent improvements to the sedimentation-erosion table. *Journal of Sedimentary Research*, 72(5), 730. <https://doi.org/10.1306/020702720730>
- Callaway, J. C., DeLaune, R. D., & Patrick, Jr. W. H. (1997). Sediment accretion rates from four coastal wetlands along the Gulf of Mexico. *Journal of Coastal Research*, 13(1), 181–191. <https://www.jstor.org/stable/4298603>
- Camporese, M., Paniconi, C., Putti, M., & Orlandini, S. (2010). Surface–subsurface flow modeling with path–based runoff routing, boundary condition–based coupling, and assimilation of multisource observation data. *Water Resources Research*, 46, W02512. <https://doi.org/10.1029/2008WR007536>
- Carbognin, L., Teatini, P., Tomasin, A., & Tosi, L. (2010). Global change and relative sea level rise at venice: What impact in term of flooding. *Climate Dynamics*, 35(6), 1039–1047. <https://doi.org/10.1007/s00382-009-0617-5>
- Carbognin, L., Teatini, P., & Tosi, L. (2004). Eustacy and land subsidence in the Venice Lagoon at the beginning of the new millennium. *Journal of Marine Systems*, 51, 345–353.
- Carminati, E., & Di Donato, G. (1999). Separating natural and anthropogenic vertical movements in fast subsiding areas: The Po plain (N. Italy) case. *Geophysical Research Letters*, 26(15), 2291–2294.
- Carniello, L., Defina, A., Fagherazzi, S., & D’Alpaos, L. (2005). A combined wind wave-tidal model for the Venice Lagoon, Italy. *Journal of Geophysical Research*, 110, F04007. <https://doi.org/10.1029/2004JF001157>
- Carniello, L., Silvestri, S., Marani, M., D’Alpaos, A., Volpe, V., & Defina, A. (2014). Sediment dynamics in shallow tidal basins: In situ observations, satellite retrievals, and numerical modeling in the Venice Lagoon. *Journal of Geophysical Research: Earth Surface*, 119, 802–815. <https://doi.org/10.1002/2013JF003015>
- Chmura, G. L., Burdick, D. M., & Moore, G. E. (2012). Recovering salt marsh ecosystem services through tidal restoration. In C. T. Roman, & D. B. Burdick (Eds.), *Tidal Salt Marsh Restoration: A Synthesis of Science and Practice* (pp. 233–751). Washington DC: Island Press. <https://doi.org/10.5822/978-1-61091-229-7-15>
- Chmura, G. L., Costanzab, R., & Kusters, E. C. (1992). Modelling coastal marsh stability in response to sea level rise: A case study in coastal Louisiana, USA. *Ecological Modelling*, 61(1), 47–64. [https://doi.org/10.1016/0304-3800\(92\)90049-K](https://doi.org/10.1016/0304-3800(92)90049-K)
- Christiansen, T., Wiberg, P., & Milligan, T. (2001). Flow and sediment transport on a tidal salt marsh surface. *Estuarine, Coastal and Shelf Science*, 50, 315–331.
- Church, J. A., Clark, P. U., Cazenave, A., Gregory, J. M., Jevrejeva, S., Levermann, A., et al. (2013). Sea Level Change. In T. F. Stocker, et al. (Eds.), *Climate Change 2013: The Physical Science Basis. Contribution of Working Group I to the Fifth Assessment Report of the Intergovernmental Panel on Climate Change* (pp. 1137–1216). Cambridge: Cambridge University Press.

- Cola, S., Sanavia, L., Simonini, P., & Schrefler, B. A. (2008). Coupled thermohydronechanical analysis of Venice lagoon salt marshes. *Water Resources Research*, *44*, W00C05. <https://doi.org/10.1029/2007WR006570>
- Costanza, R., d'Arge, R., deGroot, R., Farber, S., Grasso, M., Hannon, B., et al. (1997). The value of the World's Ecosystem Services and Natural Capital. *Nature*, *387*, 253–260.
- D'Alpaos, L. (2010). *Fatti e misfatti di idraulica lagunare*, vol. 44. Venezia, Italy: Istituto Veneto di Lettere Scienze e Arti, Memorie Scienze Fisiche.
- D'Alpaos, A., Da Lio, C., & Marani, M. (2012). Biogeomorphology of tidal landforms: Physical and biological processes shaping the tidal landscape. *Ecohydrology*, *5*(5), 550–562. <https://doi.org/10.1002/eco.279>
- D'Alpaos, A., & Marani, M. (2016). Reading the signatures of biologic-geomorphic feedbacks in salt-marsh landscapes. *Advances in Water Resources*, *93*, 265–275. <https://doi.org/10.1016/j.advwatres.2015.09.004>
- Da Lio, C., D'Alpaos, A., & Marani, M. (2013). The secret gardener: Vegetation and the emergence of biogeomorphic patterns in tidal environments. *Philosophical Transactions. Series A, Mathematical, Physical, and Engineering Sciences*, *371*(2004), 20120367. <https://doi.org/10.1098/rsta.2012.0367>
- Day, J., Rybczyk, J., Scarton, F., Rismondo, A., Are, D., & Cecconi, G. (1999). Soil accretionary dynamics, sea-level rise and the survival of wetlands in Venice Lagoon: A field and modelling approach. *Estuarine, Coastal and Shelf Science*, *49*(5), 607–628. <https://doi.org/10.1006/ecss.1999.0522>
- Deegan, L. A., Johnson, D. S., Warren, R. S., Peterson, B. J., Fleeger, J. W., Fagherazzi, S., & Wollheim, W. M. (2012). Coastal eutrophication as a driver of salt marsh loss. *Nature*, *490*, 388–392.
- Elder, J. W. (1959). The dispersion of marked fluid in turbulent shear flow. *Journal of Fluid Mechanics*, *5*(4), 544–560. <https://doi.org/10.1017/S0022112059000374>
- Fagherazzi, S., Kirwan, M. L., Mudd, S. M., Guntenspergen, G. R., Temmerman, S., D'Alpaos, A., et al. (2012). Numerical models of salt marsh evolution: Ecological, geomorphic, and climatic factors. *Reviews of Geophysics*, *50*, RG1002. <https://doi.org/10.1029/2011RG000359>
- Ferrarin, C., Ghezzi, M., Umgiesser, G., Tagliapietra, D., Camatti, E., Zaggia, L., & Sarretta, A. (2013). Assessing hydrological effects of human interventions on coastal systems: Numerical applications to the Venice Lagoon. *Hydrology and Earth System Sciences*, *17*, 1733–1748. <https://doi.org/10.5194/hess-17-1733-2013>
- French, J. R. (1993). Numerical simulation of vertical marsh growth and adjustment to accelerated sea-level rise, North Norfolk, UK. *Earth Surface Processes and Landforms*, *18*, 63–81. <https://doi.org/10.1002/esp.3290180105>
- French, J. (2006). Tidal marsh sedimentation and resilience to environmental change: Exploratory modeling of tidal, sea-level, and sediment supply forcing in predominantly allochthonous systems. *Marine Geology*, *235*, 119–136. <https://doi.org/10.1016/j.margeo.2006.10.009>
- Gambolati, G., Giunta, G., & Teatini, P. (1998). Numerical modeling of natural land subsidence over sedimentary basins undergoing large compaction. In G. Gambolati (Ed.), *CENAS - Coastline evolution of the Upper Adriatic Sea due to sea level rise and natural and anthropogenic land subsidence* (pp. 77–102). Dordrecht: Kluwer Academic Publ.
- Gambolati, G., & Teatini, P. (2013). *Venice shall rise again. Engineered uUplift of Venice through seawater injection*: Elsevier Insights. eBook ISBN 9780124201484.
- Ganju, N. K., Defne, Z., Kirwan, M. L., Fagherazzi, S., D'Alpaos, A., & Carniello, L. (2017). Spatially integrative metrics reveal hidden vulnerability of microtidal salt marshes. *Nature Communications*, *8*, 14156. <https://doi.org/10.1038/ncomms14156>
- Gibbs, R. (1985). Estuarine flocs: Their size, settling velocity and density. *Journal of Geophysical Research*, *90*, 3249–3251. <https://doi.org/10.1029/JC090iC02p03249>
- Horton, B. P., Shennan, I., Bradley, S. L., Cahill, N., Kirwan, M., Kopp, R. E., & Shaw, T. A. (2018). Predicting marsh vulnerability to sea-level rise using Holocene relative sea-level data. *Nature Communications*, *9*, 2687. <https://doi.org/10.1038/s41467-018-05080-0>
- Jankowski, K. L., Törnqvist, T. E., & Fernandes, A. M. (2017). Vulnerability of Louisiana's coastal wetlands to present-day rates of relative sea-level rise. *Nature Communications*, *8*, 14792. <https://doi.org/10.1038/ncomms14792>
- Kirwan, M., & Murray, A. (2007). A coupled geomorphic and ecological model of tidal marsh evolution. *Proceedings of the National Academy of Sciences U.S.A.*, *104*(15), 6118–6122. <https://doi.org/10.1073/pnas.0700958104>
- Lambeck, K., Antonioli, F., Anzidei, M., Ferranti, L., Leoni, G., Scicchitano, G., & Silenzi, S. (2011). Sea level change along the Italian coast during the Holocene and projections for the future. *Quaternary International*, *232*(1–2), 250–257. <https://doi.org/10.1016/j.quaint.2010.04.026>
- Lesser, G. R., Roelvink, J. A., van Kester, J. A. T. M., & Stelling, G. S. (2004). Development and validation of a three-dimensional morphological model. *Coastal Engineering*, *51*(8–9), 883–915. <https://doi.org/10.1016/j.coastaleng.2004.07.014>
- Long, A. J., Waller, M. P., & Stupples, P. (2006). Driving mechanisms of coastal change: Peat compaction and the destruction of late Holocene coastal wetlands. *Marine Geology*, *225*, 63–84.
- Marani, M., D'Alpaos, A., Lanzoni, S., Carniello, L., & Rinaldo, A. (2007). Biologically controlled multiple equilibria of tidal landforms and the fate of the Venice Lagoon. *Geophysical Research Letters*, *34*, L11402. <https://doi.org/10.1029/2007GL030178>
- Marani, M., D'Alpaos, A., Lanzoni, S., Carniello, L., & Rinaldo, A. (2010). The importance of being coupled: Stable states and catastrophic shifts in tidal biomorphodynamics. *Journal of Geophysical Research*, *115*, F04004. <https://doi.org/10.1029/2009JF001600>
- Marani, M., Da Lio, C., & D'Alpaos, A. (2013). Vegetation engineers marsh morphology through multiple competing stable states. *Proceedings of the National Academy of Sciences U.S.A.*, *110*(9), 3259–3263. <https://doi.org/10.1073/pnas.1218327110>
- Mariotti, G. (2016). Revisiting salt marsh resilience to sea level rise: Are ponds responsible for permanent land loss? *Journal of Geophysical Research: Earth Surface*, *121*, 1391–1407. <https://doi.org/10.1002/2016JF003900>
- Mariotti, G., & Fagherazzi, S. (2010). A numerical model for the coupled long-term evolution of salt marshes and tidal flats. *Journal of Geophysical Research*, *115*, F01004. <https://doi.org/10.1029/2009JF001326>
- Massey, A. C., Paul, M. A., Gehrels, W. R., & Charman, D. J. (2006). Autocompaction in Holocene coastal back-barrier sediments from south Devon, southwest England, UK. *Marine Geology*, *226*(3–4), 225–241. <https://doi.org/10.1016/j.margeo.2005.11.003>
- Morris, J. T. (2006). Competition among marsh macrophytes by means of geomorphological displacement in the intertidal zone. *Estuarine, Coastal and Shelf Science*, *69*, 395–402. <https://doi.org/10.1016/j.ecss.2006.05.025>
- Morris, J. T., & Haskin, B. (1990). A 5-yr record of aerial primary production and stand characteristics of *Spartina alterniflora*. *Ecology*, *71*(16), 2209–2217.
- Morris, J. T., Sundareswar, P. V., Nietch, C. T., Kjerfve, B., & Cahoon, D. R. (2002). Responses of coastal wetlands to rising sea level. *Ecology*, *83*, 2869–2877. [https://doi.org/10.1890/0012-9658\(2002\)083\[2869:ROCWTR\]2.0.CO;2](https://doi.org/10.1890/0012-9658(2002)083[2869:ROCWTR]2.0.CO;2)

- Mudd, S. M., D'Alpaos, A., & Morris, J. T. (2010). How does vegetation affect sedimentation on tidal marshes? Investigating particle capture and hydrodynamic controls on biologically mediated sedimentation. *Journal of Geophysical Research*, *115*, F03029. <https://doi.org/10.1029/2009JF001566>
- Mudd, S. M., Fagherazzi, S., Morris, J. T., & Furbish, D. J. (2004). Flow, sedimentation, and biomass production on a vegetated salt marsh in South Carolina: Toward a predictive model of marsh morphologic and ecologic evolution. In S. Fagherazzi, M. Marani, & L. K. Blum (Eds.), *The ecogeomorphology of tidal marshes* (pp. 165–188). Washington, DC: American Geophysical Union (AGU). <https://doi.org/10.1029/CE059p0165>
- Mudd, S. M., Howell, S. M., & Morris, J. T. (2009). Impact of dynamic feedbacks between sedimentation, sea-level rise, and biomass production on near surface marsh stratigraphy and carbon accumulation. *Estuarine, Coastal and Shelf Science*, *82*(3), 377–389. <https://doi.org/10.1016/j.ecss.2009.01.028>
- Murray, A. B., Knaapen, M. A. F., Tal, M., & Kirwan, M. L. (2008). Biomorphodynamics: Physical–biological feedbacks that shape landscapes. *Water Resources Research*, *44*, W11301. <https://doi.org/10.1029/2007WR006410>
- Paul, M. A., & Barras, B. F. (1998). A geotechnical correction for post-depositional sediment compression: Examples from the Forth valley, Scotland. *Journal of Quaternary Science*, *13*(2), 171–176. [https://doi.org/10.1002/\(SICI\)1099-1417\(199803/04\)13:2<171::AID-JQS369>3.0.CO;2-Z](https://doi.org/10.1002/(SICI)1099-1417(199803/04)13:2<171::AID-JQS369>3.0.CO;2-Z)
- Pizzuto, J. E., & Schwendt, A. E. (1997). Mathematical modeling of autocompaction of a Holocene transgressive valley-fill deposit, Wolfe Glade, Delaware. *Geology*, *25*(1), 57–60. [https://doi.org/10.1130/0091-7613\(1997\)025<0057:MMOAOA>2.3.CO;2](https://doi.org/10.1130/0091-7613(1997)025<0057:MMOAOA>2.3.CO;2)
- Roelvink, J. A. (2006). Coastal morphodynamic evolution techniques. *Coastal Engineering*, *53*(2–3), 277–287. <https://doi.org/10.1016/j.coastaleng.2005.10.015>
- Rybczyk, J. M., Callaway, J. C., & Day, J. W. Jr. (1998). A relative elevation model for subsiding coastal forested wetland receiving wastewater effluent. *Ecological Modelling*, *112*, 23–44. [https://doi.org/10.1016/S0304-3800\(98\)00125-2](https://doi.org/10.1016/S0304-3800(98)00125-2)
- Scarton, F., Rismondo, A., & Day, J. (1998). Above and belowground production of *Arthrocnemum Fruticosum* on a Venice Lagoon saltmarsh. *Bollettino del Museo civico di storia naturale di Venezia*, *48*, 237–245.
- Scarton, F., Rismondo, A., & Nascimbeni, P. (2000). Primi dati su biomassa e produzione di *Spartina maritima* (Curtis) Fernald, *Limonium serotinum* (Rchb.) Pign. e *Juncus maritimus* Lam. in Laguna di Venezia. *Società Veneziana di Scienze Naturali*, *25*, 29–35.
- Silvestri, S., Defina, A., & Marani, M. (2005). Tidal regime, salinity and salt marsh plant zonation. *Estuarine, Coastal and Shelf Science*, *62*, 119–130. <https://doi.org/10.1016/j.ecss.2004.08.010>
- Teatini, P., Gambolati, G., & Tosi, L. (1995). A new 3-D non-linear model of the subsidence of Venice. In F. B. J. Barends, F. J. J. Brouwer, & F. H. Schroder (Eds.), *Land Subsidence. Proceedings of the 5th International Symposium on Land Subsidence* (pp. 353–361). UK: IAHS Publ. NO. 234.
- Tosi, L., Teatini, P., Carbognin, L., & Brancolini, G. (2009). Using high resolution data to reveal depth-dependent mechanisms that drive land subsidence: The Venice coast, Italy. *Tectonophysics*, *474*, 271–284. <https://doi.org/10.1016/j.tecto.2009.02.026>
- van Asselen, S. (2011). The contribution of peat compaction to total basin subsidence: Implications for the provision of accommodation space in organic-rich deltas. *Basin Research*, *23*, 239–255. <https://doi.org/10.1111/i.1365-2117.2010.00482.x>
- Wolstencroft, M., Shen, Z., Törnqvist, T. E., Milne, G. A., & Kulp, M. (2014). Understanding subsidence in the Mississippi delta region due to sediment, ice, and ocean loading: Insights from geophysical modeling. *Journal of Geophysical Research: Solid Earth*, *119*, 3838–3856. <https://doi.org/10.1002/2013JB010928>
- Zecchin, M., Baradello, L., Brancolini, G., Donda, F., Rizzetto, F., & Tosi, L. (2008). Sequence stratigraphy based on high-resolution seismic profiles in the late Pleistocene and Holocene deposits of the Venice area. *Continental Shelf Research*, *29*(10), 1343–1359.
- Zhang, Y., Slingerland, R., & Duffy, C. (2016). Fully-coupled hydrologic processes for modeling landscape evolution. *Environmental Modelling & Software*, *82*, 89–107. <https://doi.org/10.1016/j.envsoft.2016.04.014>
- Zoccarato, C., Minderhoud, P. S. J., & Teatini, P. (2018). The role of sedimentation and natural compaction in a prograding delta: Insights from the mega Mekong delta, Vietnam. *Scientific Reports*, *8*, 11437. <https://doi.org/10.1038/s41598-018-29734-7>
- Zoccarato, C., & Teatini, P. (2017). Numerical simulations of Holocene salt-marsh dynamics under the hypothesis of large soil deformations. *Advances in Water Resources*, *110*, 107–119. <https://doi.org/10.1016/j.advwatres.2017.10.006>